ADVANCED MATERIALS TECHNOLOGIES
www.advmattechnol.de

A Tri-Droplet Liquid Structure for Highly Efficient Intracellular Delivery in Primary Mammalian Cells Using Digital Microfluidics

*Samuel R. Little, Ziuwin Leung, Angela B.V. Quach, Alison Hirukawa, Fatemeh Gholizadeh, Mehri Hajiaghayi, Peter J. Darlington, and Steve C.C. Shih**

Automated techniques for mammalian cell engineering are needed to examine a wide range of unique genetic perturbations especially when working with precious patient samples. An automated and miniaturized technique making use of digital microfluidics to electroporate a minimal number of mammalian cells (≈40 000) at a time on a scalable platform is introduced. This system functions by merging three droplets into a continuous droplet chain, which is called a triDrop. In the triDrop configuration, the outer droplets are comprised of high-conductive liquid while an inner or middle droplet comprising of low-conductivity liquid that contains the cells and biological payloads. In this work, it is shown that applying a voltage to the outer droplets generates an effective electric field throughout the tri-droplet structure allowing for insertion of the biological payload into the cells without sacrificing long-term cell health. This technique is shown for a range of biological payloads including plasmids, mRNA, and fully formed proteins being inserted into adherent and suspension cells which include primary T-cells. The unique features of flexibility and versatility of triDrop show that the platform can be used for the automation of multiplexed gene edits with the benefits of low reagent consumption and minimal cell numbers.

1. Introduction

Recent advances in ex-vivo cell engineering have led to new frontiers for cellular therapies.[1–3] Adding biological payloads (DNA, RNA, or protein) into a cell can supply these cells with a customized function. Specifically, in the field of immunotherapy, removing immune cells from the human body, engineering the cells, and injecting them into a patient has shown to be a robust treatment regimen for a wide range of ailments including both hematological[4,5] and solid[6,7] forms of cancer, infection,[8] and autoimmunity.[9] To further advancethe field of cellular therapy, and more specifically the field of immunotherapy, researchers need the capability to assess large arrays of genetic perturbations, allowing them to cycle through design iterations in rapid succession. To integrate any of these functions, biological payloads must be inserted into the cells, and this generally relies on three mechanisms: biological[10] (viral transduction), chemical[11] (cationic polymer, calcium phosphate, cationic lipid, or cationic amino acid), and physical[12] (electroporation, mechanoporation, sonoporation, hydrodynamic-poration, or microinjection). Concerns over immunogenicity, semi-random transgene integration, and cytotoxicity have resulted in viral transduction becoming less popular, while low transfection efficiencies have led to decreased enthusiasm for chemical techniques.[13] Physical transfection techniques are still the

S. R. Little, Z. Leung, S. C. Shih
Department of Electrical and Computer Engineering
Concordia University
Montréal, Québec H3G 1M8, Canada
E-mail: steve.shih@concordia.ca

The ORCID identification number(s) for the author(s) of this article can be found under https://doi.org/10.1002/admt.202300719

DOI: 10.1002/admt.202300719

S. R. Little, Z. Leung, A. B. Quach, S. C. Shih
Centre for Applied Synthetic Biology
Concordia University
Montréal, Québec H3G 1M8, Canada

A. Hirukawa
DropGenie
Boston, MA 02111, USA

F. Gholizadeh, M. Hajiaghayi, P. J. Darlington, S. C. Shih
Department of Biology
Concordia University
Montréal, Québec H3G 1M8, Canada

P. J. Darlington
PERFORM Center
Department of Health
Kinesiology and Applied Physiology
Concordia University
Montreal, Québec H3G 1M8, Canada

preferred approach as they generate temporary nanopores in the cell membrane allowing the cargo suspended in the surrounding media to permeate the cell where it remains trapped after the pores heal.[12]

In the last two decades, microfluidics has emerged as a leading contender for automating mammalian cell transfection[14] with several techniques excelling at the transfection of immortalized cell lines and primary T cells.[15–26] Most of these methods have relied on channel microfluidic devices for clinical manufacturing applications that require processing of large numbers of cells (>millions). However, these devices are limited in their ability to easily control unique transfection parameters in parallel or to perform transfection at smaller cell quantities which is useful for research and development. For instance, Bloemberg et al.[27] detailed the development of 15 unique chimeric antigen receptors (CARs) targeting a solid tumor-specific antigen (EGFRvIII) constructed using a rapid modular cloning strategy. After screening and testing in Jurkats, five high-performing variants were selected for insertion via viral transduction into primary T cells. To test their entire library using primary T cells, optimized electroporation protocols[28] would require upwards of 30 million cells which can be difficult to obtain from a single donor without lengthy ex vivo expansion protocols. To enable efficient screening of large libraries, such as the one created by Bloemberg et al., and to minimize the time required for cell culture and growth to reach the optimal density, an alternative approach is necessary for the efficient delivery of target payloads. This approach should allow for the use of lower cell quantities and possess the potential for parallelization and automation. Moreover, cell-based immunotherapies require inactivated primary T-cells[29] or natural killer cells or more rare immune cells such as tumor-infiltrating leukocytes,[30] or gamma-delta T cells[31] which are challenging to recover and to expand to large quantities.[32] Therefore there is much interest in working with lower number of primary immune cells, although transfecting at lower cell densities has shown to be detrimental to viability and efficiency.[28,33]

Digital microfluidics (DMF) is a droplet-based technique that relies on the generation of electrostatic forces to actuate nL-µL droplets across a grid of electrodes via application of an electric potential.[34] DMF has been used extensively for applications with mammalian cells,[35] and is also a promising platform for large-scale parallelization with simple PCB-based designs capable of handling up to 50 samples in parallel,[36] and more complex designs can handle 1000s of droplets at time.[37] In recent years, DMF has been used to automate viral transfection[38] as well as lipid-based transfection[39] using mammalian cells, however, efforts to integrate physical transfection methods such as electroporation onto a DMF platform have been limited to only microbial cells.[40,41] Both of these systems resulted in >98% of all cells dying and only 2.3%[40] or up to 9%[41] of surviving cells being successfully transfected making the proposed designs not suitable for mammalian cells due to high cell death. The two major causes of cell death using previously shown DMF electroporator designs are excessive current generation during pulsing leading to joule heating,[42] and the effects of electrochemical reactions occurring at the metallic anode and cathode leading to a pH change in the media.[43] Several channel-based microfluidic systems have rectified these problems, reducing current by creating a high-resistance electroporation environment,[44] and protecting cells from electrochemical species by isolating cells away from metallic electrodes.[20,45] To our knowledge, we are not aware of a robust method for implementing high efficiency, high viability physical transfection onto a DMF chip for mammalian cells.

In this work, we show for the first time a three-droplet assemblage for facilitating DMF electroporation, which we refer to as triDrop electroporation. The triDrop system consists of three droplets merged into a sequential chain, with the flanking droplets comprised of high conductivity media and the middle droplet comprised of low conductivity media containing cells and target payloads. Using this droplet arrangement, the platform enables superior electroporation results, compared to simpler single droplet arrangements, and we can achieve high electroporation efficiencies (>95%) with high viabilities (>95%) for a diverse range of easy-to-transfect cell types while delivering large cargo (2000 kDa FITC-tagged dextran molecules and mRNA) and complex biological cargo such as plasmids (≈5 kb) and Cas9 ribonucleic proteins for genetic engineering applications. Next, we show that the triDrop system can be used for the electroporation of primary human T cells with minimal cell numbers, high efficiency (≈90%), high viability ratios 24 h after transfection (≈90%), and with the ability to grow at rates comparable to non-electroporated samples for up to a week post-transfection. Finally, we show applications of CRISPR-Cas9 gene editing in primary human T cells by first showcasing the knockout of a well-characterized gene with up to 80% efficiency, and an automated arrayed gene editing assay where we perform 10 unique editing conditions with two replicates (totaling 20 electroporation reactions) while using fewer than one million cells from a single donor. We propose that the triDrop represents an important tool in genetic engineering that can be easily implemented into current pipelines for engineering immune cells for the development of novel cellular immunotherapies.

2. Results and Discussion

2.1. TriDrop Electroporation Using Digital Microfluidics

Figure 1a illustrates the triDrop workflow for electroporating 20 000 – 40 000 mammalian cells. This process involves several steps: sample preparation and collection, which entails preparing immortalized cell lines or primary cells extracted from a patient; resuspending the cells in electroporation buffer to achieve a concentration of at least 2×10^7 cells mL^{-1}, along with the desired payload; and loading them into the reservoirs of the DMF device. Notably, the use of low cell numbers in this workflow signifies a significant reduction in the required cell quantity when compared to existing systems. Presently, commercial platforms for primary T cell electroporation necessitate larger cell inputs, with manufacturer-recommended protocols suggesting a minimum of 200 000 cells for the Neon System (10 µL at a concentration of 2×10^7 cells mL^{-1}), and at least 1 million cells for the Lonza and Celetrix systems (20 µL at a concentration of 5×10^7 cells mL^{-1}). By employing the triDrop method, it becomes feasible to perform downstream assays such as flow cytometry and sequencing while starting with a reduced cell population.

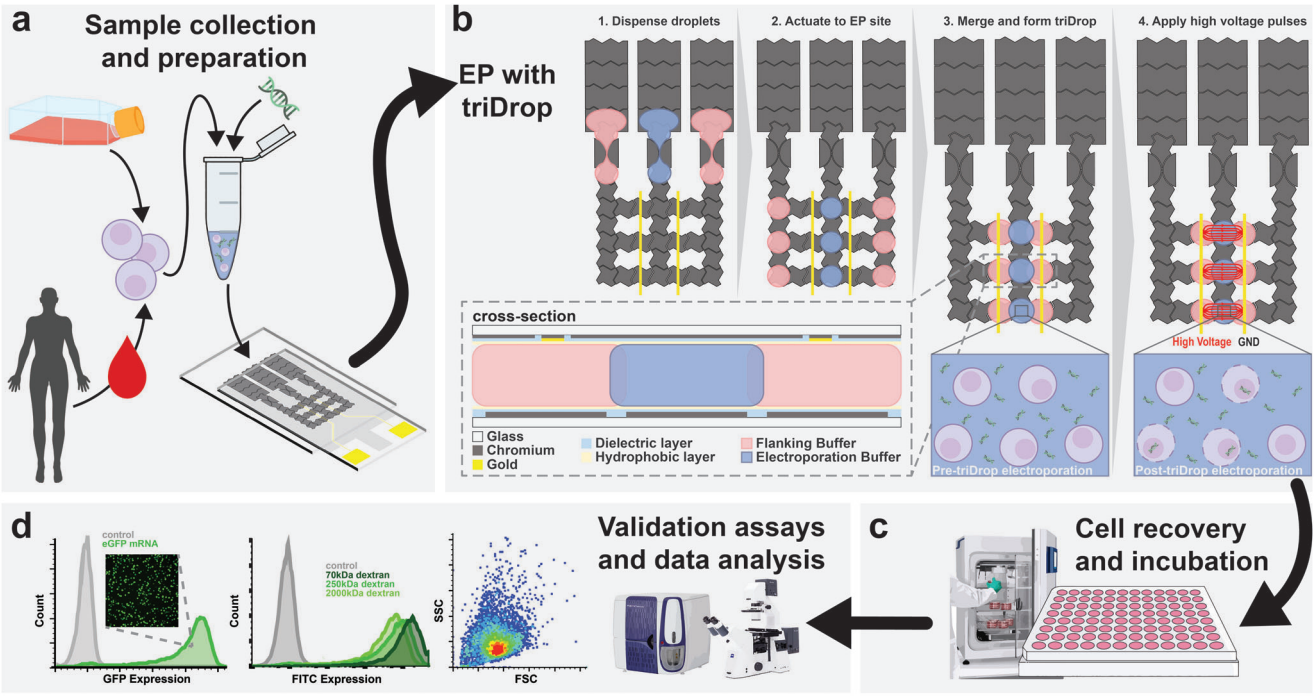

Figure 1. TriDrop platform design and overall experimental workflow for genetically engineering cells with the triDrop system. a) Cell sample was cultured and prepared by resuspending it in an electroporation buffer with target delivery molecules. b) The schematic illustration shows top-view of the DMF device and the formation of the triDrop through a series of electrode actuation. The red lines (in frame 4) indicate the electric field lines generated during application of high-voltage pulses. The inset shows the cross-sectional view of the triDrop. c) After electroporation, samples were then incubated (>24 h) for cell recovery and followed by d) analysis using FACS or with fluorescent microscopy or any analytical method of interest.

The triDrop instrument is comprised of multiple components (Figure S1, Supporting Information): the DMF device for the droplet manipulations, our imaging setup for visualizing the droplets on the device, an electroporation pulse circuit, and a DMF actuation circuit with open-source code (see BitBucket registry in Methods). The DMF device is comprised of two plates: the bottom plate, which contains the reservoir and driving electrodes to create the triDrop structure, and the top plate, which contains Au-lines for applying the electroporation pulses to the triDrop structure as well as the grounding plane for the DMF driving voltage. The droplets sandwiched between the plates are comprised of either high or low-conductivity buffers containing mammalian cells and various payloads for delivery. Once the samples are loaded, the triDrop structure can be formed easily using our previously shown DMF platform[38,46] which allows for complete automation of all dispensing, actuation, and merging as well as automating the application of programmable high voltage pulses for electroporation.

The process of triDrop electroporation is shown in Figure 1b. A key feature of the system is the use of low cell numbers – users can input a low number of cells 20 000 to 40 000 cells per reaction for efficient transfection. Upon inputting cells into the reservoirs, three 1 µL droplets were dispensed, actuated to an electroporation site, and merged into a sequential chain as shown in Figure 1b (hereby referred to as the triDrop structure). Within the triDrop structure, the inner droplet (hereby referred to as the sample droplet) was comprised of low conductivity media ($\sigma \approx 8$ mS cm^{-1}) and contained mammalian cells in suspension along with the payload to be delivered into the cells (in our work, the payloads used are dextran molecules of various sizes, mRNA, plasmids, or Cas9 proteins). The outer droplets (hereby referred to as the liquid electrodes) were comprised of high conductive media ($\sigma \approx 16$ mS cm^{-1}) and were in contact with gold electrodes fabricated into the device top plate and provide an electrical connection between the metal electrodes and the sample droplet, similar to forming a liquid electroporation cuvette. After merging the three droplets into the triDrop structure, mixing was limited to diffusion and the structure consisted of three discrete regions for over 30 s post-merge (Figure S2a, Supporting Information), which allowed time for delivering high-voltage pulses to the gold electrodes and electroporating the cells. The electroporation process was complete within 5 s of droplet merging and the total time for triDrop implementation from reservoir loading to electroporation was ≈3 min for three triDrop structures (Supplementary Video). Immediately after electroporation, cells were loaded off-chip for post-electroporation culture for up to 7 days (Figure 1c) and were analyzed using microscopy, flow cytometry and validated with fluorescent-based assays (Figure 1d). To our knowledge, the triDrop system shows state-of-the-art transfection efficiency with exceptional viability throughout and is the first technique shown for scalable mammalian cell electroporation on DMF devices and joins a small collection of microfluidic devices capable of transfecting primary human immune cells.[15–26]

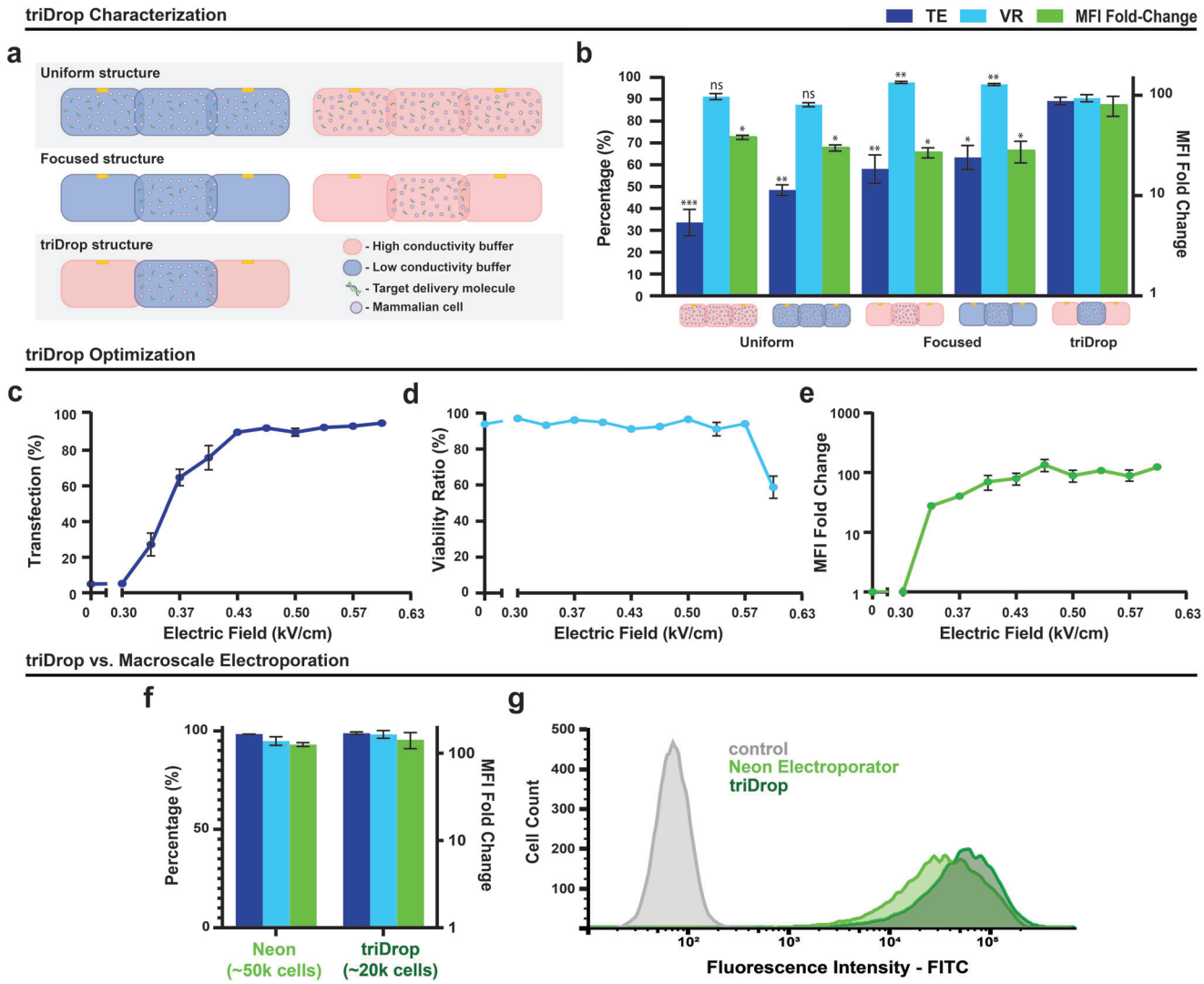

Figure 2. System characterization and optimization for triDrop electroporation with HEK293 cells. a) Illustrations showing different droplet liquid structures used for electroporation characterization. Pink droplets represented high conductivity media ($\sigma \approx 16$ mS cm^{-1}) and blue droplets represent low conductivity media ($\sigma \approx 8$ mS cm^{-1}). b) Plots showing transfection efficiency (TE; dark blue), viability ratio (VR; light blue) and mean fluorescence intensity (MFI) fold-change (green) for five different droplet electroporation structures when inserting a 70 kDa FITC-tagged dextran molecule. Significance markers ($p < 0.05$, $n = 3$) are in reference to the triDrop arrangement. Plots showing the c) transfection efficiency, d) viability ratio, and e) MFI fold-change with respect to the applied electric field using the triDrop system for the insertion of 70 kDa FITC-tagged dextran molecule into HEK293 cells. The statistical analysis was performed via an ordinary one-way ANOVA ($n = 3$). Graphical representation showing the f) efficiency, viability ratio, and MFI fold-change for the Neon (standard) versus the triDrop system. These quantitative values were obtained from g) the cell counts displaying FITC fluorescence from electroporated and non-electroporated samples from the Neon system and the triDrop. SEM are calculated based on $n = 3$. n.s indicated no significant difference, *, **, and *** represent p-Values below 0.05, 0.01, and 0.001 respectively. Statistical analysis was performed using an ordinary one-way ANOVA.

2.2. Characterization of the triDrop System

In initial experiments, we explored the use of co-planar electrodes paired with various droplet structures to generate a sufficient electric field to insert 70 kDa FITC-tagged dextran into the easy-to-transfect HEK293 cell line. The droplet structures tested here are shown in **Figure 2**a and described as follows: 1) a uniform structure – one homogenous 3 µL droplet comprised of either high or low conductivity medium with the cells and payload distributed homogenously throughout, 2) a focused structure – three 1 µL droplets comprised of the same media that are merged together with only the middle droplet containing cells and payload, and 3) a triDrop structure – two droplets of high conductivity buffer flanking a droplet with low conductivity buffer containing cells and payload. Three, 200 V_{DC} pulses, 10 ms in duration (determined via numerical simulations) were applied to the droplet structures, and the results were analyzed using three metrics, transfection efficiency (TE), viability ratio (VR), and mean fluorescence intensity (MFI) fold change. Figure 2b shows that the triDrop structure has significantly higher TE

(89%) and MFI fold change (79) than any of the other droplet structures while still maintaining a viability ratio of >90% ($p < 0.05$, $n = 3$). Additionally, we show that the success of the triDrop structure can be recreated without a significant difference when the middle droplet is comprised of another low conductivity electroporation buffer ($\sigma \approx 7.4$ mS cm^{-1}) but not when using high conductivity electroporation buffers (σ >15 mS cm^{-1}) (Figure S3, Supporting Information). To understand the experimental results above, we developed a COMSOL simulation of the uniform and triDrop structure described in Figure S4 (Supporting Information), and the results shown in Figures S5 and S6 (Supporting Information). The simulation of the uniform structure shows the outer regions of the structure experience electric fields that are low for mammalian electroporation (< 0.2 kV cm^{-1}),[47] regions close to the gold electrodes have a high but inconsistent electric field (≈0.7 kV cm^{-1}), and the middle section of the droplet structure has a homogenous electric field that is too low for electroporation (0.35 kV cm^{-1}). Comparing this to the simulation of the triDrop structure shown in Figure S6c (Supporting Information), forming the outer droplets using high conductive media and the inner droplet using low conductivity media results in a homogenous electric field (0.55 kV cm^{-1}) that focuses across the middle of the triDrop structure, solving the problem of heterogenous electric field generation that has plagued other droplet electroporation systems.[48] In the triDrop configuration, all the cells (which are entirely located in the middle droplet) experience a consistent electric field while being exposed to a significantly lower current than common benchtop systems (≈30 mA vs 3000 mA)[49] (Figure S7, Supporting Information). This is an important result because isolating the cells in the middle of the droplet structure will prevent harmful electrochemical species (generated at the metal-liquid interface)[50] from changing the pH of the cell media and negatively affecting the health of the cells (see images of pH test in Figure S2b, Supporting Information). Given these observations, the triDrop structure offers optimal results compared to the uniform or focused liquid structures when using identical electroporating conditions.

We hypothesized that the three quantitative metrics (TE, VR, and MFI-fold change) for the triDrop structure might be improved by varying the applied electric field. To test this hypothesis, a range of electric fields were applied to determine the optimal field for inserting 70 kDa FITC-tagged dextran molecules into HEK293 cells. These data, shown as line graphs in Figure 2c-e, confirm that there is range of fields (0.5-0.63 kV cm^{-1}) to achieve excellent TE (≈ 90%), VR (≈ 90%), and MFI fold change (>80). Repeating this optimization for Jurkat and HeLa cells (Figure S8, Supporting Information) reveals a slightly higher effective range (0.75-0.90 kV cm^{-1}). These applied fields place us within the expected range reported by other high-performance electroporation devices.[20,44] A list of all electroporation conditions tested throughout this study and the corresponding parameters can be found in Table S1 (Supporting Information).

To evaluate the triDrop method relative to gold standard practices (Neon transfection system), a series of transfections were performed using HeLa cells and dextran as the payload. All pulse parameters for triDrop are identical to those described above and the Neon was operated using the manufacturer-recommended settings. The key differences between the systems are that the cell numbers used for the triDrop were lower than the Neon and sample volumes for transfection were reduced. When working with HeLa cells the Neon requires 10 µL of sample at a concentration of 5×10^6 cells mL^{-1} (50 000 total cells) whereas the triDrop requires only 1 µL at a concentration of 2×10^7 cells mL^{-1} (20 000 total cells). As shown in Figure 2f, cells transfected with the triDrop show very similar high metrics as the Neon (TEs >98%, VRs >95% and MFI fold change >125). The transfection efficiency was calculated by flow cytometry analysis with the results of the FITC fluorescence counts (for ≈15 000 events) to be very similar for both systems (but different than the non-electroporated control cells) (Figure 2g). These experiments show that our technique can achieve similar metrics as the standard mammalian-based transfection system with lower cell numbers. As described below, these low cell numbers enabled our work with primary T-cells, which are usually difficult to transfect when cell numbers are below 1×10^6 cells since their post-electroporation viability decreases significantly.[28,33]

2.3. Immortalized Cells

To further evaluate the capacity to transfect mammalian cells, different payloads were delivered to three commonly used immortalized cell types: HEK293, HeLa, and Jurkat cells. Each set of cells was prepared and loaded into the DMF platform (as in Figure 1b) and was transfected with four different payloads: 70, 250, and 2000 kDa FITC-tagged dextran, and a 5 kb eGFP plasmid. **Figure 3**a,b shows the quantitative metrics for the typical model transfection cell line HEK293 and HeLa cells for the three different dextran sizes (along with a non-electroporated control) respectively. As shown, the metrics are excellent, with a TE >90% (left-side *y*-axis), VR >90% (left-side *y*-axis), and >80 MFI fold-change (right-side *y*-axis). In fact, the triDrop system was able to insert the large 2000 kDa FITC-tagged dextran molecule (hydraulic diameter ≈ 55 nm)[51] into both HEK293 and HeLa cell lines with a TE and VR of >90%. These results show that the delivery of large molecules into the cytosol of HEK293 and HeLa cells using triDrop is efficient and suggests that the system will be capable of delivering fully formed proteins of similar size or other large molecules.[25]

Moving towards a more biologically relevant payload, we performed the same protocol for delivering plasmids. Figure 3c shows the TE and VR for HEK293 and HeLa cells, as shown, we obtained a TE and VR of 71% and 90% for HEK293 and 60% and 99% for HeLa with both cell types showing healthy morphology after transfection (Figure S9, Supporting Information). These results were obtained via flow cytometry and ≈15 000 cell events were collected for each sample and the frequency fluorescence histogram is depicted in Figure 3d (HEK293) and Figure 3e (HeLa). In both cases, the control population showed very minimal fluorescence (see grey histogram) while the eGFP positive cells (showing successful triDrop electroporation) were shifted towards higher fluorescence than the control (see green plots). We note that plasmid transfection poses a greater challenge as it requires nuclear delivery rather than just cytosolic delivery. Consequently, the delivery rates of plasmids are often lower compared to dextran molecules or mRNA molecules.[52,53] Regardless, these data confirm the triDrop system can be used to insert both large payloads as well as biological payloads which have been

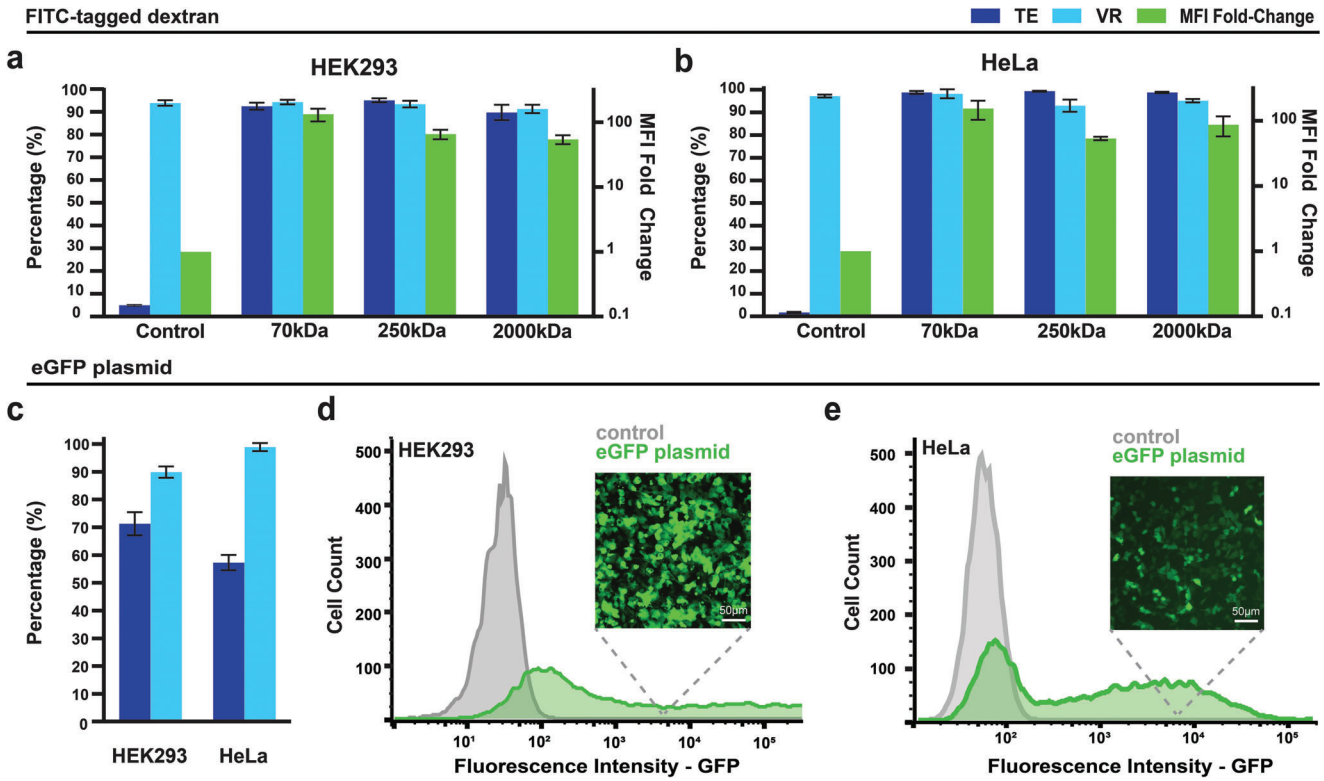

Figure 3. Intracellular delivery of diverse payloads in HEK293 and HeLa cells using triDrop electroporation. Plots of transfection efficiency, viability ratio, and MFI fold-change comparing an un-electroporated control vs the triDrop system for the insertion of 70, 250, and 2000 kDa FITC-tagged dextran molecules for a) HEK293 cells and b) HeLa cells. c) Plots of transfection efficiency and viability ratio for HEK293 and HeLa when inserting an eGFP plasmid. Fluorescence intensity histograms showing GFP expression for d) HEK293 cells and e) HeLa cells vs a non-electroporated control. Inset shows fluorescence images of (d) HEK293 cells and (e) HeLa cells expressing the eGFP plasmid. All plots with error bars are based on standard error of the mean for $n = 3$ replicates.

challenging to deliver for other microfluidic-based mammalian transfection devices.[54]

Next, we tested our system with Jurkat T-cells since they have been shown to be a suitable model in immunotherapy research[27] and have a reputation for being more difficult to transfect cell lines.[55] Here, we followed the same protocol as above – electroporating three different dextran molecules (70, 250, and 2000 kDa), and eGFP plasmid. Additionally, we included an mRNA payload given the increasing interest to use mRNA as an immunotherapeutic molecule.[56] **Figure 4**a shows the dextran results for our three metrics are quantitatively similar to HEK293 and HeLa – VR and TE >90%. The flow cytometry histogram (Figure 4b) shows a full spectral shift towards higher fluorescence intensities for all three dextran sizes confirming that we can efficiently insert large molecules into Jurkat cells with minimal effect on viability. Furthermore, we transfected a 1 kb eGFP mRNA and a 5 kb eGFP plasmid. Figure 4c shows results 24 h post-transfection with the mRNA displaying an impressive TE of 95% (measured via frequency histogram Figure 4d), a VR of 98%, and an MFI fold-change of >500 while using only 2 pico grams of mRNA per cell. Electroporation with both payloads did not negatively influence the morphology of the cells (Figure S9, Supporting Information), however, the plasmid (measured 48 h post-transfection) showed a modest TE of 40% (measured via frequency histogram Figure 4e), and a VR of 96% and a very modest MFI fold-change of ≈12. Taken together, these data suggest that the triDrop technique is suitable for both types of payloads for Jurkat cell transfection, with mRNA having higher TE, similar to previous microfluidic transfection works.[18]

As a final proof-of-principle in Jurkat cells, the triDrop system was used for an on-chip CRISPR knock-out of the β-2-microglobulin (β2M) gene. The β2M gene codes for a protein that serves as a key structural element in all major histocompatibility (MHC) class 1 molecules[57] and when the gene is impaired it can no longer form and be expressed on the cell surface making this an ideal target for an easily detectable proof-of-concept knockout. Jurkat cells were mixed with a Cas9 RNP containing either a scrambled gRNA or a gRNA targeting the β2M gene and loaded on to the chip for triDrop electroporation, immediately post electroporation cells were moved off-chip and into recovery buffer and left to incubate for 72 h. After recovery, cells were blocked for non-specific binding and then stained with a FITC-tagged antibody targeting MHC class 1 molecules. Figure 4f depicts histogram data for the three different conditions – control (no triDrop electroporation, grey line), non-targeting gRNA (triDrop electroporation with a scrambled gRNA, blue line), and β2M targeting gRNA (triDrop electroporation with a β2M specific gRNA, green line). All three populations had high

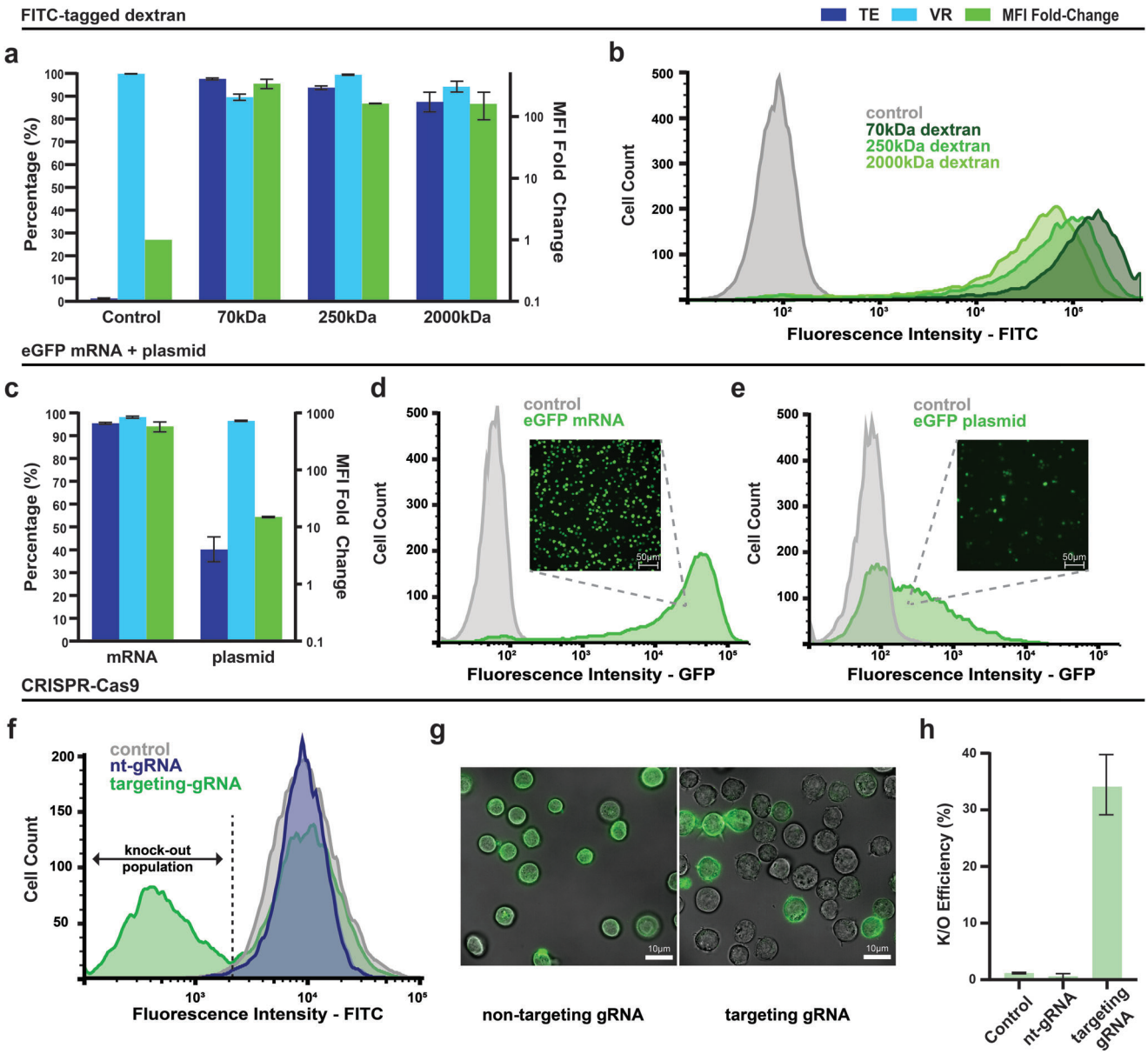

Figure 4. Intracellular delivery of diverse payloads into Jurkat cells using triDrop electroporation. a) Plots of transfection efficiency, viability ratio, and MFI fold-change comparing a non-electroporated control vs the triDrop system for the insertion of a 70, 250, and 2000kDa FITC-tagged dextran molecules. b) Fluorescence intensity histograms showing the FITC expression comparing the control with the three different dextran molecules inserted using the triDrop system. c) Plots of transfection efficiency, viability ratio, and MFI fold-change for the insertion of eGFP-mRNA, and eGFP-plasmid using the triDrop system. Fluorescence intensity histograms showing GFP expression for d) eGFP-mRNA and e) eGFP-plasmid inserted using triDrop electroporation vs. a non-electroporated control. Inset shows fluorescence images for cells expressing (d) eGFP-mRNA and (e) eGFP-plasmid. f) Fluorescence intensity histograms showing the FITC expression comparing a control vs. non-targeting gRNA vs β2M targeting gRNA populations after staining with a FITC-tagged anti-β2M antibody. g) Fluorescence images overlaid with bright field images showing (left) cells electroporated with a non-targeting (nt) gRNA and (right) cells electroporated with a gRNA targeting the β2M gene and stained with a FITC-tagged anti-β2M antibody. h) Plots of β-2-microglobulin knockout efficiency comparing a non-electroporated control vs. cells electroporated with a Cas9 protein conjugated with a non-targeting gRNA vs. cells electroporated with a Cas9 protein conjugated with a gRNA targeting the β-2-microglobulin gene. All plots with error bars are based on standard error of the mean for $n = 3$ replicates.

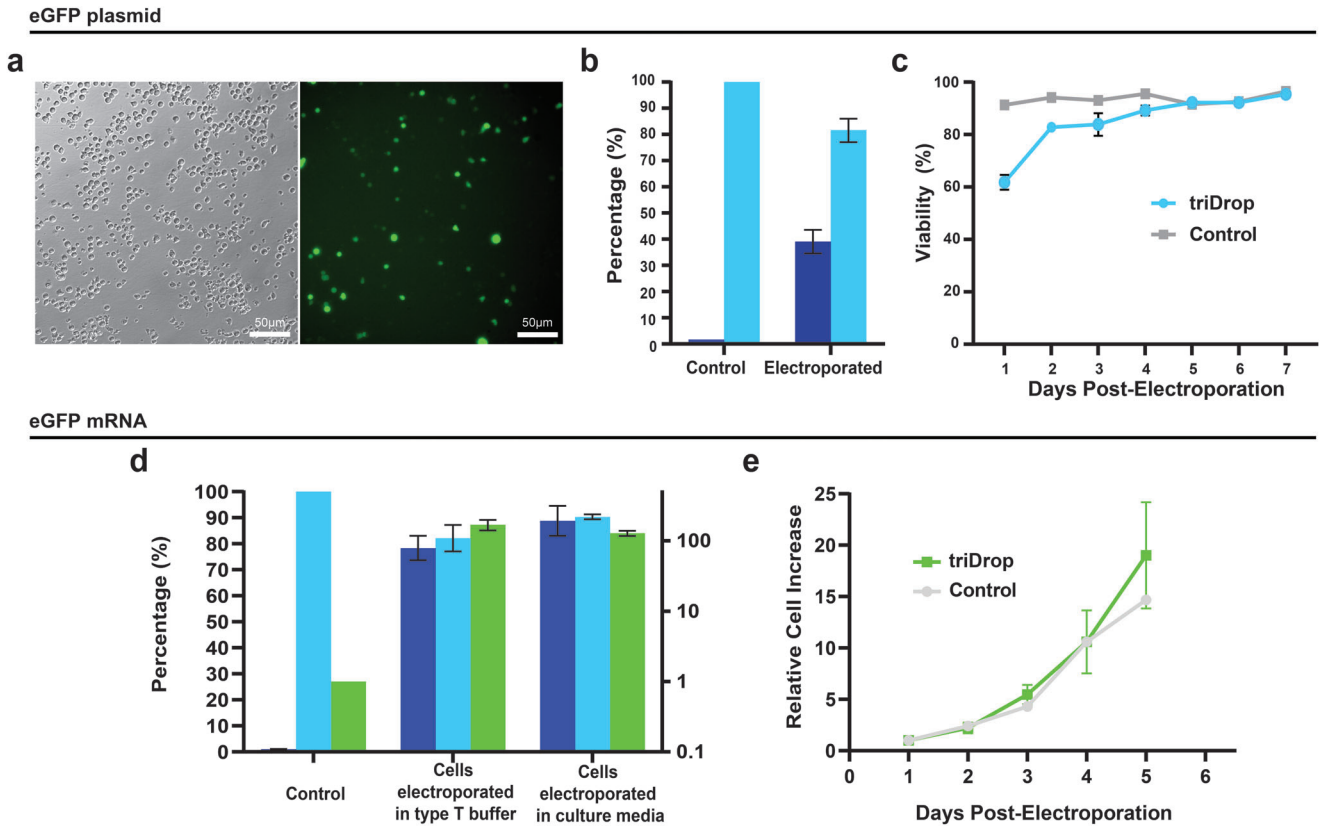

Figure 5. Intracellular delivery of valuable payloads into human primary CD4+ T cells using triDrop electroporation. a) bright-field (left) and fluorescence (right) images showing GFP expression 48 h post electroporation with the triDrop system. b) Plots of transfection efficiency and viability ratio comparing an un-electroporated control vs the triDrop system for the insertion of a 5kb eGFP plasmid 48 h post-transfection. c) Viability measurements for 7 days of post-electroporation culture comparing a non-electroporated control vs. the triDrop system. d) Plots of transfection efficiency, viability ratio, and MFI fold-change comparing samples electroporated with different electroporation buffers. e) The cell increase of samples relative to day 1 for 7 days of post-electroporation for samples electroporated vs. non-electroporated control. All plots with error bars are based on standard error of the mean for $n = 3$ replicates.

viabilities (≈95%), however, only cells that were electroporated with the β2M specific gRNA show a knockout population which is represented by cells with a lower fluorescence intensity (i.e., a peak is shown on the left of the dotted line). As illustrated in representative images after staining, cells remain healthy after 72 h (≈ 95% viability) and only those with knocked out β2M show cells with no fluorescence (Figure 4g). The knockout efficiency is summarized in Figure 4h and shows an average knockout efficiency of 35% for the cells electroporated with the β2M targeting gRNA whereas the two control populations both have < 2% knockout. In sum, the gene-editing application here shows that the triDrop platform can deliver complex payloads into mammalian cells.

2.4. Primary T cells

With the rise of immunotherapy showing promise for cancer patients, much research has been put into transfecting primary T cells.[58] While Jurkat cells can provide promising initial indicators for immunotherapies, final tests must be done in primary human immune cells.[27] Currently, there is no technology that is capable of generating libraries of engineered primary T cells in an automated and arrayed fashion without requiring millions of cells. To demonstrate the high-impact applicability of the triDrop system, we demonstrate the transfection process for primary human CD4+ T cells.

We first optimized the triDrop electroporation protocol for the insertion of the 2000 kDa dextran payload. Given the sensitive nature of these cells, we explored reducing the pulse duration as this parameter is known to have a significant effect on cell viability.[47] For each condition, three, 450 V pulses were applied with a duration of 1 ms, 3 ms, or 10 ms. As shown in Figure S10a–d (Supporting Information), reducing the pulse duration (1 and 3 ms) was found to have the optimal metrics with 3 ms yielding the highest TE while still yielding VRs >90%. The system was further assessed with a plasmid payload. The representative images of the cells after 48 h post-transfection with an eGFP plasmid show healthy morphology and cells producing eGFP (**Figure 5**a). The electroporated cells were compared to cells that were not electroporated via flow cytometry histograms (Figure S10e,f, Supporting Information). We quantified the VR as well as the TE, and as shown in Figure 5b, the triDrop electro-

porated cells show a VR of 81% and a TE >38%. These are good metrics for plasmid delivery into primary T cells comparing modestly with some commercially available systems such as the Neon (64% TE and 94% viability),[59] the Lonza system (70% TE, 60% viability),[60] or the Celetrix system (40% TE, 50% viability).[28] The viability of electroporated cells were monitored daily for the one-week post-electroporation and compared against a non-electroporated control. It was observed that the health of the electroporated cells is comparable to that of non-electroporated cells by day 5 (Figure 5c) and, 7 days post electroporation, both the control population and the electroporated population had viabilities >95% (also shown by the forward and side scatter plots – Figure S10g, Supporting Information).

In addition, we show the delivery of eGFP mRNA using cell culture media as our electroporation buffer. The deleterious effects of long-term exposure to electroporation buffer on mammalian cells are well-documented[61] and many buffer manufacturers recommend minimizing the time cells spend in the buffer. Furthermore, proprietary electroporation buffers can be prohibitively expensive.[62] A unique feature of our triDrop system is the ability to generate the electric field focusing effect on a wide variety of different media if the flanking droplets are comprised of a higher conductivity solution. We created a very high conductive solution ($\sigma \approx 32$ mS cm^{-1}, recipe in Tables S2 and S3, Supporting Information) to use as a flanking buffer for primary T cells suspended in RPMI ($\sigma \approx 15$ ms cm^{-1}) to maintain the high-low-high buffer conductivity triDrop structure. Figure 5d shows a comparison between cells electroporated in low conductivity buffer with the original triDrop configuration compared to cells electroporated in culture media using the very high conductive flanks. Both conditions show impressive results, however, as predicted, the cells electroporated in the culture media had superior VR (90% vs 82%) and higher TE (89% vs 78%). The electroporated cells were allowed to grow out for 5 days post-electroporation and were found to proliferate at a rate comparable to that of non-electroporated cells. After 5 days of culture electroporated cells and control cells show a similar fold increase with a ≈19 and ≈15-fold population increase respectively (Figure 5e). Compared to four recent high-performance microfluidic transfection systems[18,20,21,63] for the insertion of mRNA into primary human T cells, the triDrop can achieve the best percentage of cells that are both living and transfected while using the least amount of mRNA per cell (Figure S11, Supporting Information).

Finally, we showcase our triDrop system for CRISPR-Cas9 gene editing in primary human CD4+ T cells. First, we performed a knockout targeting a well-established β2M gene. **Figure 6**a depicts histogram data for a non-electroporated condition (grey line), a condition electroporated with a non-targeting gRNA (blue line), and a condition electroporated with a β2M-targeting gRNA (green line). All cells were stained with a FITC-tagged anti-β2M antibody four days post-electroporation. As expected, the control condition and the condition electroporated with a non-targeting gRNA show complete expression of the β2M protein, however, the condition electroporated with the targeting gRNA show a significant leftward shift indicating substantially reduced β2M expression (i.e., reduced fluorescence). In addition, Figure 6b shows that after four days post-electroporation, the triDrop system (and the editing) has no observable impact on cell health when compared to the control condition as determined by staining with DAPI. We also measured the knockout efficiency for these three conditions, and as shown in Figure 6c, the targeted β2M gRNA shows an average knockout efficiency of 70%, which is similar to previously shown microfluidic gene editing systems when targeting this gene in primary cells.[64]

The final assay was motivated by widespread interest in performing arrayed gene editing on primary T cells for immunotherapeutic discovery.[65] We combined the triDrop gene editing capabilities with our DMF platform's capacity for parallelized automation to perform an automated, 5-plex arrayed gene editing experiment. As a model system, we targeted the knockout of the T cell receptor alpha constant (TRAC) locus due to the recent interest in using this site for T cell receptor therapies.[66] The device and method shown in Figure 6d were designed with additional sample reservoirs to hold cells suspended in low-conductivity electroporation buffer mixed with one of the unique guide conditions and additional electroporation sites to increase parallel processing. Four gRNAs were designed (sequence in Table S4, Supporting Information) and arranged into 10 unique conditions to target the TRAC locus as summarized in Figure 6e. To perform this experiment, we followed the same protocol as before except for using a chip capable of performing five unique triDrop electroporations in parallel (Figure S12, Supporting Information). Generally, these types of multiplexed experiments require at least 200 000 cells per condition,[64] however, for our experiments (20 total electroporation reactions), fewer than 1 million cells from a single donor were used for all conditions. Figure 6f summarizes the knockout results as measured via flow cytometry 4 days post-electroporation. As expected, all conditions had knockout efficiencies significantly different than the non-targeting and the control ($p < 0.05$), with each condition achieving at least 30% average knockout. Interestingly, cells electroporated with multiple gRNAs had significantly higher knockout efficiencies than cells electroporated with only one gRNA ($p < 0.001$, Figure S13, Supporting Information), and the full combination of all four gRNAs together had the highest average knockout (67%) which is inline with previously shown results.[67] Histogram plots depicting TCR expression with the best result from each condition are shown in Figure 6g. These results show that triDrop electroporation can be combined with high throughput DMF automation to perform arrayed CRISPR experiments with high-value cell lines.

The capability to perform electroporation at these lower cell numbers is a significant challenge with current commercially available techniques, rather these systems are required to use at least ≈ 200 000 cells, and usually between 1–2 million cells per condition when working with sensitive cell lines. TriDrop is an efficient technique with excellent viabilities and transfection efficiencies (>90%) for immortalized and primary cells alike while requiring only 40 000 cells for a single reaction. Moreover, we have shown that the triDrop system can be combined with DMF for a simple arrayed CRISPR screen while using fewer than one million primary human T cells, and we hope in the future this capability can be expanded to test large libraries of novel constructs on rare cells. This capability will accelerate the pace of immune cell engineering, requiring less time and resources to grow and culture cells during research and

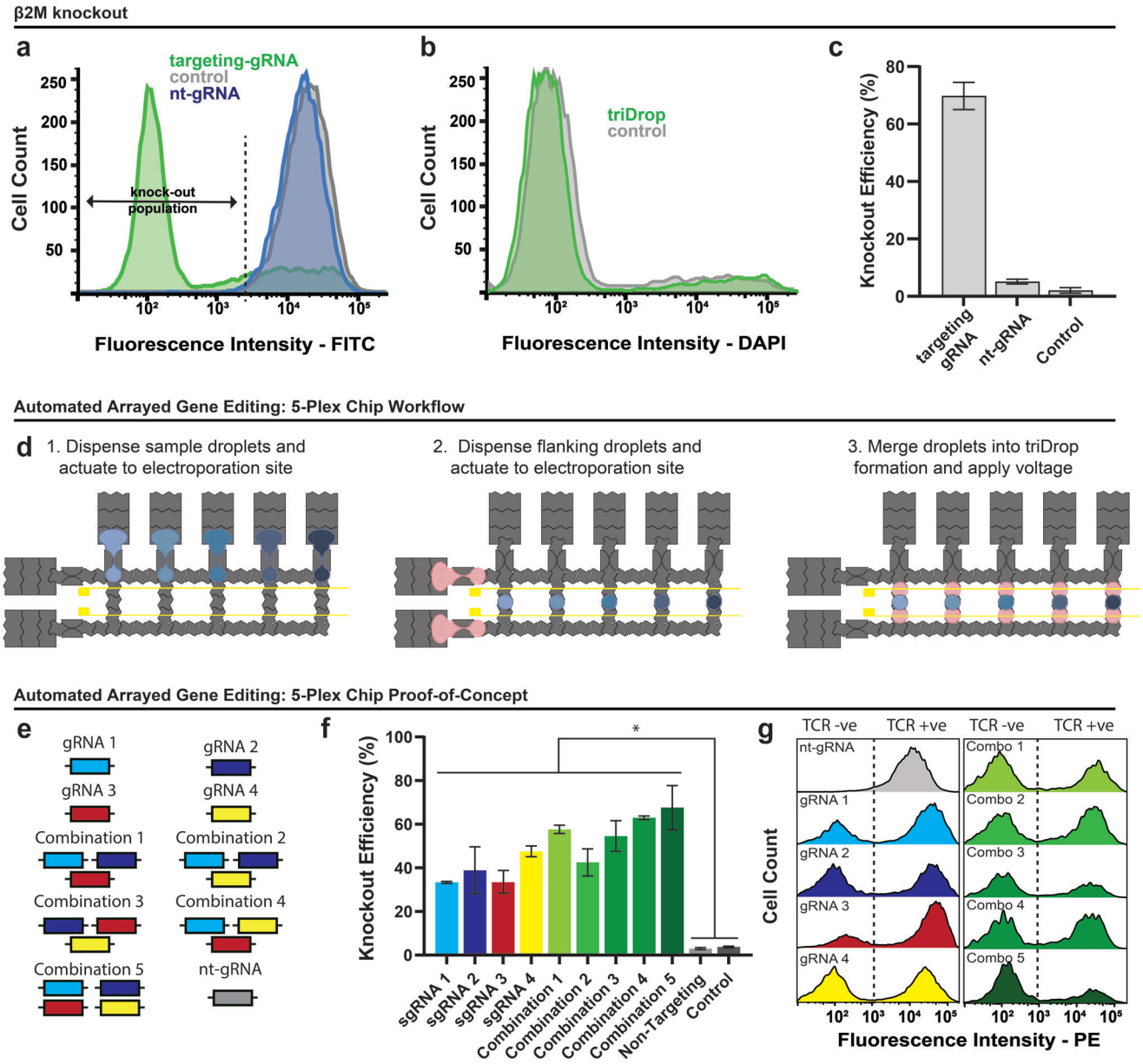

Figure 6. CRISPR-Cas9 gene editing applications in human primary CD4+ T cells using triDrop electroporation. a) Fluorescence intensity histograms showing the FITC expression comparing a control vs. non-targeting gRNA vs β2M targeting gRNA populations after staining with a FITC-tagged anti-β2M antibody. b) Fluorescence intensity histograms showing the DAPI staining comparing a control vs. electroporated population after four days of culture. c) β2M knockout efficiency summary for three conditions. d) Schematic illustrations showing the operations of an automated DMF platform capable of the simultaneous electroporation of 5 unique samples. e) Summary of all conditions for the arrayed automated gene editing experiment. f) Summary of TRAC-knockout efficiency for all 10 conditions plus a non-electroporated control. g) Fluorescence intensity histograms showing TCR expression for all 10 analyzed conditions. Error bars are based on standard error of the mean for (c) $n = 3$ replicates and (f) $n = 2$ replicates. * Represents p-values below 0.05. Statistical analysis was performed using an unpaired t-test.

development stages, while also making it more affordable due to less consumption of expensive reagents like Cas9 proteins and gRNAs. We believe the triDrop system will help lift barriers in immune cell engineering and open the door to discovering new therapeutic breakthroughs via high throughput arrayed screening.

3. Conclusion

We show for the first time the ability to perform highly efficient and highly viable electroporation of immortalized and primary mammalian cells on a DMF platform using a tri-droplet liquid structure. Moreover, our platform can work with low quantities

of mammalian cells, which can be cost-efficient and expedite the engineering workflow for mammalian cells. We compared our system with the Neon system and showed very comparable transfection results. Additionally, as an application, we described results relating to performing five unique CRISPR edits in parallel while using the human primary T cells. We propose such a platform would be potentially integrated with other DMF devices for end-to-end automation of mammalian cell engineering[68] similar to what has been shown previously for microbial cells[68,70] and be used for applications related to the field of genome editing and cell-based immunotherapies.

4. Experimental Section

Reagents and Materials: Unless specified otherwise, general-use chemicals and kits were purchased from Sigma-Aldrich (St. Louis, MO). Device fabrication reagents and supplies included chromium-coated glass slides, and gold-coated glass slides with AZ1500 photoresist from Telic (Valencia, CA), MF-321 positive photoresist developer from Rohm and Haas (Marlborough, MA), chromium etchant 9051 and gold etchant TFA from Transene (Danvers, MA), AZ-300T photoresist stripper from AZ Electronic Materials (Somerville, NJ), Teflon-AF 1600 from DuPont Fluoroproducts (Wilmington, DE). Transparency masks for device fabrication were printed from ARTNET Pro (San Jose, CA) and polylactic acid (PLA) material for 3D printing was purchased from 3Dshop (Mississauga, ON, Canada). General chemicals for tissue culture were purchased from Wisent Bio Products (Saint-Bruno, QC, Canada). eGFP plasmid (Figure S14, Supporting Information) and mRNA (Table S4, Supporting Information for sequences) for this study were acquired from Addgene (catalog: 54767) and TriLink Biotechnologies (catalog: L-7201) respectively. Electronic components were obtained from DigiKey (Thief River Falls, MI). Electroporation buffers were obtained from Harvard Apparatus Canada (St Laurent, QC), Thermo Fisher Scientific (Burlington, ON), or made in-house (see Table S3, Supporting Information). Neon transfection reagents were purchased from Thermo Fisher Scientific (Burlington, ON).

TriDrop Device Fabrication and Setup: TriDrop devices, each comprising a bottom plate with Cr-based electrodes and a top-plate with Au-based electroporation electrodes, were fabricated at Concordia's cleanroom facility using transparent photomasks printed at 25 400 dpi (Artnet Pro, Bandon, OR). An overview of the fabrication process is illustrated in Figure S15 (Supporting Information). DMF bottom plates bearing chromium electrodes coated with a SU-8 5 dielectric and Teflon-AF hydrophobic layer were formed using a previously outlined methodology.[71] Each bottom plate features an array of 30 actuation electrodes (2 mm by 2 mm), 12 reservoir electrodes (2.9 mm by 5.5 mm) arranged into 3 reservoirs, 6 active dispensing electrodes (2 mm by 2 mm), and 3 splitting electrodes (3.8 mm × 3 mm). The electrode array has inter-electrode gaps of 150 mm and each electrode was connected to a pogo-pin holder.

TriDrop top plates bearing gold electrodes (0.2 mm wide) were formed from a glass substrate coated with 100 nm gold adhered to a seed chromium layer (≈12 nm). To form the gold electrodes, top plates were spin-coated (10 s 500 rpm, 30 s 3000 rpm, 20 s 5000 rpm) in S1811, exposed through a transparent mask, developed using Microposit MF321 (2 min), washed with DI water, submerged in gold etchant (2 min), washed with DI water, and submerged in AZ stripper to remove the remaining photoresist before being washed with acetone, IPA, and DI water, and dried with nitrogen. To disconnect the chromium from the gold wiring, we followed the above protocol except using CR-4 etchant to remove the chromium. To insulate the gold electroporation electrodes from the Cr-grounding layer, the top plate was surface treated for 45 s in a plasma cleaner (Harrick Plasma PDC-001, Ithaca, NY) before coating a 5 µm dielectric of SU8-5. Briefly, the photoresist was spin-coated (10 s 500 rpm, 30 s 2500 rpm), followed by a soft bake (65 °C 2 min, 95 °C, 10 min), exposed to UV light through a custom mask (5 s), post-exposure baked (65 °C 2 min, 95 °C 10 min), developed in SU8 developer (15 s), rinsed with IPA and DI water, dried with nitrogen, and then hard baked (180 °C, 10 min). Bottom plates were spin-coated with Teflon-AF 1600 in 2% w/w in Fluorinert FC-40 (10 s 500rpm, 30s 1500rpm). To assemble the completed triDrop device, the top and bottom plates were assembled using two layers of double-sided tape (180 µm total thickness, 3M), and the gold electrode on the top plate was aligned directly above electroporation sites on the bottom plate.

Cell Culture: HeLa and HEK293 cells were cultured in Dulbecco's Modified Eagle Medium (DMEM) and Jurkat cells in RPMI-1640 (kindly provided by Prof. Alisa Piekny, Concordia). All media contained 10% heat-inactivated fetal bovine serum (FBS) and 100 U mL^{-1} penicillin/streptomycin. Cells were passaged every 2–3 days and maintained in a humidified chamber at 37 °C with 5% CO_2. For triDrop experiments, HeLa and HEK293 cells were passaged by first washing with PBS, then trypsinizing with 0.25% trypsin-EDTA followed by washing with DMEM before seeding cells in a fresh flask at 2×10^5 cells mL^{-1}. Jurkat cells were passaged by centrifuging at 300 g for 5 min to pellet the cells, aspirating the media, and resuspending in RPMI before seeding at 1×10^5 cells mL^{-1}. Prior to electroporation, aliquots of 600 000 cells were prepared and resuspended with target molecules in EP buffer to a final volume of either 15 µL or 30 µL.

Primary human CD4+ T cells were either purchased from BPS bioscience (catalog #79752, San Diego, CA) or separated from fresh primary blood and purified using EasySep Human CD4 T cell Isolation kit to a purity of 95% (STEMCELL Technologies, Canada, Catalog # 17952) (Figure S16, Supporting Information). All cells were kept in liquid nitrogen prior to use. For experiments with plasmid, mRNA, and dextran, cells were thawed and cultured in a complete culture medium consisting of RPMI-1640 with 10% FBS, 100 U mL^{-1} penicillin/streptomycin, and 100 IU mL^{-1} recombinant human IL-2 (Fisher Scientific Ottawa, ON). After 24 h, the cells were activated with Human T-Activator CD3/CD28 Dynabeads (Fisher Scientific Ottawa, ON, #11131D) and were incubated for up to 48 h. After incubation, activator beads were removed following the manufacturer's protocol by first gently pipetting up and down to release cells from the activator beads followed by transferring the cells to a magnetic tube rack for 1–2 min to allow for cells and beads separation and the supernatant containing cells was transferred to a fresh tube. Primary T cells were counted using TC20 Automated Cell Counter (BioRad, CA) and maintained at 1×10^6 cells mL^{-1} by daily addition of complete culture media. Prior to electroporation, cell aliquots of 600 000 cells were prepared and resuspended with target molecules with EP buffer to a final volume of 15 µL for each unique condition. For gene editing experiments with primary T cells, culture conditions were adapted from Roth et al.[33] Briefly, cells were thawed into culture media supplemented with, 10% FBS, 200 IU mL^{-1} IL-2, 10 ng mL^{-1} IL-7 (Peprotech, cat no: 200–07), and 5 ng mL^{-1} IL-15 (Peprotech, cat no: 200–15). Post-electroporation cells were recovered in the same media cocktail but with IL-2 levels increased to 500 IU mL^{-1}.

Bulk Electroporation: Prior to electroporation, HeLa cells were seeded the day before transfection (day 0) to reach 70–80% confluency by day 1. Immediately before electroporation, adherent cells were trypsinized (using 0.25% trypsin-EDTA), washed, re-suspended in media, and counted with TC20 Automated Cell Counter (BioRad, CA). The Neon transfection system (Thermo Fisher) was then used to electroporate cells using the manufacturer's protocol following four steps: 1) cells were centrifuged at 300 g for 3 min and washed with 500 µL PBS before being resuspended 5×10^6 cells mL^{-1} in the Neon electroporation buffer. 2) FITC-tagged dextran molecules were then added to a final concentration of 300 µg mL^{-1}. 3) the electroporation sample was mixed (via gentle up-and-down pipetting) and transferred to the Neon capillary electroporation tip and was electroporated using the parameters recommended by the manufacturer for HeLa (1005 V, 2 pulses, 35 ms), and 4) immediately after electroporation, cells were placed into a six-well plate containing 2 mL of pre-warmed culture media for cell recovery. Cells were only maintained in their proprietary electroporation buffer for a maximum duration of 20 min to preserve cell viability.

TriDrop Automation and Operation: The bottom plate of the triDrop device was placed on a pogo pin holder that has been propped to a height 20 cm above the benchtop using a chassis constructed from

T-slotted aluminum extrusions purchased from McMaster-Carr (catalog #: 47065T101, Aurora, OH) and machined and assembled in-house. The system is connected to a 720-pixel, 30 frames-per-second camera (Skybasic, Houston TX.) to visualize droplet movements on the device (Figure S1, Supporting Information). A 12-input card edge connector from Digikey (catalog #: 151-1410-ND, Thief River Falls, MI), was attached to the top plate of the triDrop device and connected via three leads (DMF ground, High Voltage DC, DC ground). Two DC leads were connected to an electroporation pulse circuit (Figure S1, Supporting Information) and one lead was used to provide the electrical connection for the DMF ground. The electroporation circuit consisted of an 8-pin optocoupler (Model #: AQW216EH) purchased from Digikey was connected to a Z650-0.32-U DC power source (TDK-Lambda) and controlled by an Arduino Uno running a custom pulse generating program, creating custom pulses of varying amplitudes and durations (100 – 450 V_{DC}, 1–10 ms in duration). For automating droplet movement on the device, see the previously published work for circuit and connectivity.[46] The electroporation and DMF actuation circuit were controlled by our in-house software which is available on our bitbucket registry (https://bitbucket.org/shihmicrolab/littleleung_2023). Droplet movements were programmed by application of AC potentials (300 – 400 V_{RMS}) at 15 kHz between the top and bottom plates. The DMF actuation software was also used to initiate the electroporation pulse circuitry to ensure immediate and uniform pulse application after triDrop merging.

TriDrop Electroporation: Prior to a triDrop experiment, HEK293, HeLa, Jurkat, and primary T-cells were centrifuged at 300 g for 3 min, washed twice with a custom 1SM buffer, and resuspended in Type T electroporation buffer. For experiments using dextran molecules, cells, and dextran molecules were prepared at a final concentration of 2×10^7 cells mL^{-1} and 0.03 ng/cell respectively. For experiments with eGFP plasmid or mRNA, the payload was added to the cell sample to achieve a concentration of 1.275 and 2 pg per cell respectively, with a final cell concentration of 4×10^7 cells mL^{-1}. For CRISPR knock-out experiments, per 1 million cells,100 pmol of sgRNA and 50 pmol of Cas9 were mixed and incubated at room temperature for 10 min to allow for the formation of Cas9 RNP. The Cas9 RNP was then immediately used or stored on ice until use, where it was then added to cells in an electroporation buffer for a final concentration of 4×10^7 cells mL^{-1}.

TriDrop operation included four droplet operations and was implemented using the triDrop automation system described previously. The four steps include: 1) reservoir filling, 2) triDrop dispensing, 3) triDrop merging, and 4) triDrop electroporation. Droplet operation can be visualized in the Supplementary Video. The device consisted of three reservoirs: two outer reservoirs were filled with PBS containing 0.05% Pluronics F-68 (which we refer to as high conductivity buffer, $\sigma \approx 16$ mS cm^{-1}) and the middle reservoir was filled with cells and the desired payload suspended in electroporation buffer containing 0.05% Pluronics F68 surfactant. Reservoirs were filled by pipetting 6 µL each onto the bottom plate at the edge of the top plate and applying driving potentials to the three reservoir electrodes to draw the fluids into the reservoir. Next, ≈1 µL single droplet was dispensed from each reservoir by pulling and necking the liquid out of the reservoir using a modified droplet dispensing system.[72] The cell-containing droplet was actuated to the center of the electroporation site and the two high-conductive droplets were actuated to the outer edges of the electroporation site. The three droplets were merged by actuating the high conductive droplets towards the cell containing droplet creating a continuous three-droplet structure. Immediately upon merging, the electroporation circuit was automatically triggered to deliver a sequence of high-voltage DC square-wave pulses to the exposed Au-electrodes (on the top plate) that were in direct contact with the PBS droplets (see Table S1, Supporting Information for triDrop electroporation parameters). For experiments using the uniform electroporation arrangement, all three reservoirs contained the same media with cells and payload suspended in either electroporation buffer or PBS with 0.05% Pluronics F-68 surfactant. For experiments using the focused electroporation arrangement, all three reservoirs contain the same media (either electroporation buffer or PBS with 0.05% Pluronics F68 surfactant), however, only the middle reservoir contains cells and payload.

Immediately after triDrop electroporation, the top plate is removed, and the electroporated cells (total volume ≈ 3 µL) were immediately removed from the chip via pipetting and placed in a well plate that was pre-loaded with warmed culture media. HEK293 and HeLa cells were cultured in flat bottom 48 well plates post-electroporation for cell recovery. Jurkat and Primary T cells were cultured in a U-bottom 96 well plate post-electroporation for cell recovery. All experiments with cells were incubated for a maximum time of 20 min in an electroporation buffer to preserve optimal cell health.

Arrayed Gene Editing: An optimized gRNA design tool available from Synthego was used to design four unique gRNAs targeting the TRAC locus and were purchased from Synthego (see Table S4, Supporting Information for sequences). The four unique guides were arranged into 10 unique combinations: four individual guides, four conditions containing any three gRNA combinations, one combination containing all four guides, and one non-targeting gRNA. Prior to reservoir filling on the device, all guide combinations were prepared in equal parts: 0.9 µL of each gRNAs (100 pmol $µL^{-1}$) combined with 1.2 µL of a Cas9 protein (30 pmol $µL^{-1}$) and were incubated for 10 min to form the RNP complex. 4 µL of primary T-cells (see Cell Culture section for preparation) in type T electroporation buffer of a density 4×10^7 cells mL^{-1} were mixed with 0.6 µL of the RNP complex in a PCR tube for each combination. Immediately after preparation, cells and the RNP complex solution as well as the high conductivity were loaded onto the device following the reservoir filling protocol above. TriDrop electroporation and post-electroporation procedures followed the protocol described above.

pH Measurements: Following previously established methods for analyzing pH change in microfluidic electroporators,[43] DMF reservoirs were loaded with either high conductivity buffer (flanking reservoirs) or low conductivity media with HEK293 cells at a concentration of 2×10^7 cells mL^{-1} (middle reservoir) containing either phenolphthalein or Congo red to test the pH changes above 9.0 and between 3 – 5.2, respectively. The triDrop structure was formed following the procedure described above and 3, 200 V pulses 10 ms in duration were applied. Images of the droplets were taken every 1 s for 30 s using a wireless digital microscope (Skybasic, Houston, TX) to monitor color changes in the middle droplet.

Current Measurements: Electrical current was measured by placing a 100 Ω shunt resistor in series and downstream of the triDrop top plate. An oscilloscope was connected across the shunt resistor and the voltage peak was recorded across the resistor during an application of the electric potential (after forming the triDrop structure). The system current was determined using the Ohm's law relationship ($I_{measured} = V_{peak}/100\ \Omega$).

Flow Cytometry: Viability, transfection efficiency (TE) and mean fluorescent intensity (MFI) were measured using a BD FACS Melody (BD Bioscience, Canada). The FACS was equipped with three excitation lasers (405, 488, and 561 nm) in a 2B-2V-4YG configuration. For all experiments with dextran molecules, plasmids, or mRNA, cells were resuspended in 500 µL of culture media, washed by centrifuging (300 g, 5 min), and then resuspended in 1 mL FACS buffer (1x PBS, 1 mM EDTA, 25 mM HEPES, 1% FBS, pH 7.0), then centrifuged (300 g, 5 min), aspirated, and resuspended in 600 µL of FACS buffer. For all samples, viability was assessed by staining dead cells using 0.6 µL of DAPI (50 ng $µL^{-1}$) added to the sample immediately prior to FACS and mixed thoroughly with the sample by pipetting. Dextran, plasmids, and mRNA were excited by a 488 nm laser and viewed through a 527/32 filter. DAPI was used as an indicator for dead cells and was excited by a 405 nm laser. Our gating protocol is shown in Figure S17 (Supporting Information). Briefly, a non-electroporated control containing a payload was prepared using the above method and loaded into the FACS machine. First, the data was analyzed by comparing forward scatter and side scatter to identify which data points are cells. Next, the cell population was analyzed comparing side scatter height and side scatter width to identify singlets. Once singlets were identified, a histogram plot was generated for DAPI staining – separating living cells (DAPI negative) from dead cells (DAPI positive). Finally, the living cell population was used to generate a histogram showing FITC expression and this histogram was used to define the lower boundary of transfection with the gate being set to include ≈1% of the control population as transfected to account for endocytosis.

For each condition, 15 000 events were collected at a rate of 100 events s^{-1}.

For CRISPR gene knockout experiments, cells were maintained in culture for 72 h post-electroporation. Following maintenance, the cells were centrifuged (300 g, 5 min) and resuspended in 50 µL of culture media. 48 µL of culture media and 2 µL of Human TruStain FcX (Fc Receptor Blocking Solution, BioLegend catalog #: 422301) were mixed to prevent non-specific binding followed by 5 min of incubation at room temperature. After blocking, cells were spun down at 300 g for 5 min with the supernatant removed, resuspended in 98 µL of culture media plus 2 µL of FITC anti-human HLA-A,B,C Antibody (BioLegend catalog #: 311403), and incubated for an additional 20 min in the dark at 4 °C. After staining, the cells were then washed twice in 1 mL of FACS buffer, centrifuged (300 g, 5 min) to remove the supernatant, and resuspended in 600 µL of FACS buffer. Similar to above, FACS gates are determined by running a non-electroporated control to define normal β2M expression, and electroporated samples are compared against the control.

Post-Electroporation Analysis: FACS data was analyzed using FlowJo (Ashland, OR). After gating out the doublets and cell debris, the viability was measured as the percentage of living cells (DAPI negative) from a sample. The viability ratio (VR) was then calculated as the ratio of the viability of electroporated sample to the non-electroporated cells (i.e., control).

$$VR = \frac{Viability_{electroporated}}{Viability_{Unelectroporated}} \times 100 \quad (1)$$

TE was calculated as the number of fluorescent living cells above the threshold divided by the total number of living cells.

$$TE = \frac{number\ of\ transfected\ living\ cells}{total\ number\ of\ living\ cells} \times 100 \quad (2)$$

The background fluorescence of the cells was defined by using samples with cells only with no electroporation.

MFI fold-change was calculated by measuring the mean fluorescent intensity for non-transfected control cells as shown previously.[18] This parameter measures a relative increase in fluorescence intensity (i.e., brightness) compared to a control.

$$MFI\ fold-change = \frac{MFI_{transfected\ cells}}{MFI_{untransfected\ cells}} \quad (3)$$

Relative cell increase was calculated by dividing the cell count on each day post-electroporation by the cell count from day 1 post-electroporation. The cell count was calculated by measuring the cell centration using T20 Automated Cell Counter (BioRad, CA) and the volume of culture medium in each well.

Knockout efficiency was determined by dividing the number of living cells below a fluorescence threshold by the total number of living cells.

$$Knockout\ Efficiency = \frac{number\ of\ living\ cells\ below\ fluorescence\ threshold}{total\ number\ of\ living\ cells} \times 100 \quad (4)$$

For visual analysis, 48 h post electroporation, bright field and fluorescent images were taken a with 20x objective on an Olympus IX73 inverted microscope (Olympus Canada, Mississauga, ON, Canada) and a 100× objective on a Zeiss Axio Observer 7 with an excitation wavelength of 480 nm and a 470/40 nm excitation and 525/50 nm emission filter set (catalog # 49002, Chroma Technology Corporation, Bellows Falls, VT). The brightness and contrast of images were adjusted using ImageJ.

Statistical Analysis: Statistical analysis was performed using an ordinary one-way ANOVA with Prism V8.4 (GraphPad) with $n = 3$ replicates for Figure 2 and Figure S3 (Supporting Information). For Figure 2, an *f*-value of 13.7, 20.73, and 6.4 was obtained for transfection efficiency, viability ratio, and mean fluorescence intensity, respectively with a Dfn of 4 and Dfd of 10. For Figure S3 (Supporting Information), an *f*-value of 97.23, 4.08, and 11.36 was obtained for transfection efficiency, viability ratio, and mean fluorescence intensity, respectively with a Dfn of 3 and Dfd of 8. For Figure 6 statistical analysis was performed using an unpaired t-test.

Study Participants: All study participants gave informed consent, were recruited, and had blood drawn in compliance with relevant ethical regulations under the approved summary protocol form 30009292 at Concordia University.

Supporting Information

Supporting Information is available from the Wiley Online Library or from the author.

Acknowledgements

The authors would like to thank the lab of Dr. Alisa Piekny and Dr. Michael Sacher for the generous donation of cells and cell culturing discussions. The authors thank the Natural Sciences and Engineering Research Council (NSERC), the Canadian Foundation of Innovation (CFI), MEDTEQ+, and DropGenie Inc. for funding. S.R.L. thanks NSERC CGS-D for funding. S.R.L. and Z.L. thank NSERC CREATE SynBioApps and Concordia University Department of Electrical and Computer Engineering for FRS funding. S.C.C.S. thanks Concordia University for a Research Chair.

Conflict of Interest

S.R.L, A.H., and S.C.C.S. are co-inventors on a patent application related to the triDrop structure (Systems and methods for applying voltages within droplet-based systems; PCT US2022/032083) that describes the liquid structures for transfection reported here. The remaining authors declare no competing interests.

Author Contributions

S.R.L. and Z.L. contributed equally to this work. The novel electroporation system was designed by S.R.L., A.H., and S.C.C.S. The experiments were designed by S.R.L., Z.L., and S.C.C.S. All experiments and analyses were conducted by S.R.L. and Z.L. Biological and microfluidic methods and DMF control software were developed by S.R.L. and Z.L. Mathematical modeling and simulations were designed and performed by Z.L. Electroporation control circuits and software were designed and built by S.R.L., F.G., M.H., and P.J.D. developed the methodology for cell isolation and freezing from fresh blood and F.G. and M.H. performed the isolation and freezing protocols. All authors wrote, revised, and reviewed the manuscript.

Data Availability Statement

The data that support the findings of this study are available from the corresponding author upon reasonable request.

Keywords

cellular engineering, digital microfluidics, gene-editing, multiplex, transfection

Received: May 8, 2023
Revised: July 5, 2023
Published online:

[1] J. A. Doudna, E. Charpentier, **2014**, 346.
[2] R. Barrangou, J. A. Doudna, *Nat. Biotechnol.* **2016**, *34*, 933.
[3] J. A. Doudna, *Nature* **2020**, *578*, 229.
[4] D. W. Lee, J. N. Kochenderfer, M. Stetler-Stevenson, Y. K. Cui, C. Delbrook, S. A. Feldman, T. J. Fry, R. Orentas, M. Sabatino, N. N. Shah, S. M. Steinberg, D. Stroncek, N. Tschernia, C. Yuan, H. Zhang, L. Zhang, S. A. Rosenberg, A. S. Wayne, C. L. Mackall, *Lancet* **2015**, *385*, 517.
[5] C. H. June, M. Sadelain, *N. Engl. J. Med.* **2018**, *379*, 64.
[6] U. Patel, J. Abernathy, B. N. Savani, O. Oluwole, S. Sengsayadeth, B. Dholaria, *EJHaem* **2022**, *3*, 24.
[7] F. Marofi, R. Motavalli, V. A. Safonov, L. Thangavelu, A. V. Yumashev, M. Alexander, N. Shomali, M. S. Chartrand, Y. Pathak, M. Jarahian, S. Izadi, A. Hassanzadeh, N. Shirafkan, S. Tahmasebi, F. M. Khiavi, *Stem Cell Res Ther* **2021**, *12*, 1.
[8] Z. Jiang, H. Liang, H. Pan, et al., *Front Microbiol* **2021**, *12*, 1.
[9] Z. Mukhatayev, Y. O. Ostapchuk, D. Fang, I. C Le Poole, *Autoimmun Rev.* **2021**, *20*, 102761.
[10] E. Senís, C. Fatouros, S. Große, E. Wiedtke, D. Niopek, A.-K. Mueller, K. Börner, D. Grimm, *Biotechnol. J.* **2014**, *9*, 1402.
[11] L. Zhang, P. Wang, Q. Feng, N. Wang, Z. Chen, Y. Huang, W. Zheng, X. Jiang, *NPG Asia Mater* **2017**, *9*, 441.
[12] A. K. Fajrial, Q. Q. He, N. I. Wirusanti, J. E. Slansky, X. Ding, *Theranostics* **2020**, *10*, 5532.
[13] T. K. Kim, J. H. Eberwine, *Anal. Bioanal. Chem.* **2010**, *397*, 3173.
[14] J. Hur, A. J. Chung, *Adv. Sci.* **2021**, *8*, 2004595.
[15] J. Hur, I. Park, K. M. Lim, J. Doh, S.-G. Cho, A. J. Chung, *ACS Nano* **2020**, *14*, 15094.
[16] J. A. Jarrell, B. J. Sytsma, L. H. Wilson, F. L. Pan, H. W. J Katherine, G. Lau, A. A. Lievano, *bioRxiv* **2021**, *3*, 6.
[17] J. Loo, B. Chang, T. Dunn, O. Kim, S. Han, A. Zamarayeva, T. Sulchek, M. C. Garcia, *Sci. Rep.* **2021**, *11*, 1.
[18] B. Joo, J. Hur, G.-B. Kim, S. G. Yun, A. J. Chung, *ACS Nano* **2021**, *15*, 12888.
[19] V. Jayasooriya, B. Ringwelski, G. Dorsam, D. Nawarathna, *Lab Chip* **2021**, *21*, 3748.
[20] C. A. Lissandrello, J. A. Santos, P. Hsi, M. Welch, V. L. Mott, E. S. Kim, J. Chesin, N. J. Haroutunian, A. G. Stoddard, A. Czarnecki, J, R. Coppeta, D. K. Freeman, D. A. Flusberg, J. L. Balestrini, V. Tandon, *Sci. Rep.* **2020**, *10*, 1.
[21] J. A. Jarrell, A. A. Twite, K. H. W. J. Lau, M. N. Kashani, A. A. Lievano, J. Acevedo, C. Priest, J. Nieva, D. Gottlieb, R. S. Pawell, *Sci. Rep.* **2019**, *9*, 1.
[22] T. Ditommaso, J. M. Cole, L. Cassereau, J. A. Buggé, J. L. S Hanson, D. T. Bridgen, B. D. Stokes, S. M. Loughhead, B. A. Beutel, J. B. Gilbert, K. Nussbaum, A. Sorrentino, J. Toggweiler, T. Schmidt, G. Gyuelveszi, H. Bernstein, A. Sharei, *Proc Natl Acad Sci U S A* **2018**, *115*, E10907.
[23] G. L. Szeto, D. Van Egeren, H. Worku, A. Sharei, B. Alejandro, C. Park, K. Frew, M. Brefo, S. Mao, M. Heimann, R. Langer, K. Jensen, D. J. Irvine, *Scient. Rep.* **2015**, *5*, 10276.
[24] J. Li, B. Wang, B. M. Juba, M. Vazquez, S. W. Kortum, B. S. Pierce, M. Pacheco, L. Roberts, J. W. Strohbach, L. H. Jones, E. Hett, A. Thorarensen, J.-B. Telliez, A. Sharei, M. Bunnage, J. B. Gilbert, *ACS Chem. Biol.* **2017**, *12*, 2970.
[25] A. Sharei, R. Trifonova, S. Jhunjhunwala, G. C. Hartoularos, A. T. Eyerman, A. Lytton-Jean, M. Angin, S. Sharma, R. Poceviciute, S. Mao, M. Heimann, S. Liu, T. Talkar, O. F. Khan, M. Addo, U. H. Von Andrian, D. G. Anderson, R. Langer, J. Lieberman, K. F. Jensen, *PLoS One* **2015**, *10*, 0118803.
[26] X. Han, Z. Liu, Y. Ma, K. Zhang, L. Qin, *Adv. Biosyst.* **2017**, *1*, 1600007.
[27] D. Bloemberg, T. Nguyen, S. Maclean, A. Zafer, C. Gadoury, K. Gurnani, A. Chattopadhyay, J. Ash, J. Lippens, D. Harcus, M. Pagé, A. Fortin, R. A. Pon, R. Gilbert, A. Marcil, R. D. Weeratna, S. Mccomb, *Mol Ther Methods Clin Dev* **2020**, *16*, 238.
[28] Z. Zhang, S. Qiu, X. Zhang, W. Chen, *BMC Biotechnol.* **2018**, *18*, 1.
[29] S. Ghassemi, J. S. Durgin, S. Nunez-Cruz, J. Patel, J. Leferovich, M. Pinzone, F. Shen, K. D. Cummins, G. Plesa, V. A. Cantu, S. Reddy, F. D. Bushman, S. I. Gill, U. O'doherty, R. S. O'connor, M. C. Milone, *Nat. Biomed. Eng.* **2022**, *6*, 118.
[30] C. A. Chamberlain, E. P. Bennett, A. H. Kverneland, I. M. Svane, M. Donia, Ö. Met, *Mol Ther Oncolytics* **2022**, *24*, 417.
[31] M. Rozenbaum, A. Meir, Y. Aharony, O. Itzhaki, J. Schachter, *Front. Immun.* **2020**, *11*, 1347.
[32] T. M. Hulen, C. A. Chamberlain, I. M. Svane, Ö. Met, *Immuno* **2021**, *1*, 194.
[33] T. L. Roth, C. Puig-Saus, R. Yu, E. Shifrut, J. Carnevale, P. J Li, J. Hiatt, J. Saco, P. Krystofinski, H. Li, V. Tobin, D. N. Nguyen, M. R. Lee, A. L. Putnam, A. L. Ferris, J. W. Chen, J.-N. Schickel, L. Pellerin, D. Carmody, G. Alkorta-Aranburu, D. Del Gaudio, H. Matsumoto, M. Morell, Y. Mao, M. Cho, R. M. Quadros, C. B. Gurumurthy, B. Smith, M. Haugwitz, S. H. Hughes, et al., *Nature* **2018**, *559*, 405.
[34] K. Choi, A. H. C. Ng, R. Fobel, A. R. Wheeler, *Annu. Rev. Anal. Chem.* **2012**, *5*, 413.
[35] I. Barbulovic-Nad, H. Yang, P. S. Park, A. R. Wheeler, *Lab Chip* **2008**, *8*, 519.
[36] Y. Xing, Y. Liu, R. Chen, Y. Li, C. Zhang, Y. Jiang, Y. Lu, B. Lin, P. Chen, R. Tian, X. Liu, X. Cheng, *Lab Chip* **2021**, *21*, 1886.
[37] S. Anderson, B. Hadwen, C. Brown, *Lab Chip* **2021**, *21*, 962.
[38] A. B. V. Quach, S. R. Little, S. C. C. Shih, *Anal. Chem.* **2022**, *94*, 4039.
[39] H. Sinha, A. B. V. Quach, P. Q. N. Vo, S. C. C. Shih, *Lab Chip* **2018**, *18*, 2300.
[40] A. C. Madison, M. W. Royal, F. Vigneault, L. Chen, P. B. Griffin, M. Horowitz, G. M. Church, R. B. Fair, *ACS Synth. Biol.* **2017**, *6*, 1701.
[41] J. A. Moore, M. Nemat-Gorgani, A. C. Madison, M. A. Sandahl, S. Punnamaraju, A. E. Eckhardt, M. G. Pollack, F. Vigneault, G. M. Church, R. B. Fair, M. A. Horowitz, P. B. Griffin, *Biomicrofluidics* **2017**, *11*, 014110.
[42] M.-P. Rols, Handbook of Electroporation, **2017**, 1449.
[43] Y. Li, M. Wu, D. Zhao, et al., *Sci. Rep.* **2015**, *5*, 1.
[44] J. A. Kim, K. Cho, M. S. Shin, W. G. Lee, N. Jung, C. Chung, J. K. Chang, *Biosens. Bioelectron.* **2008**, *23*, 1353.
[45] T. Zhu, C. Luo, J. Huang, C. Xiong, Q. Ouyang, J. Fang, *Biomed. Microdevices* **2010**, *12*, 35.
[46] J. M. Perry, G. Soffer, R. Jain, S. C. C. Shih, *Lab Chip* **2021**, *21*, 3730.
[47] J. W. Pollard, Y. Luqmani, A. Bateson, K. Chotai, *Nucleic Acids* **2003**, *130*, 321.
[48] Y. Zhan, J. Wang, N. Bao, C. Lu, *Anal. Chem.* **2009**, *81*, 2027.
[49] D. J. Im, S.-N. Jeong, *Biochem. Eng. J.* **2017**, *122*, 133.
[50] G. Saulis, R. Lapė, R. Pranevičiūtė, D. Mickevičius, *Bioelectrochemistry* **2005**, *67*, 101.
[51] L. Lebrun, G.-A. Junter, *J Memb Sci* **1994**, *88*, 253.
[52] H. Bai, G. M. S. Lester, L. C. Petishnok, D. A. Dean, *Biosci. Rep.* **2017**, *37*, 20160616.
[53] D. Dean, D. Strong, W. Zimmer, *Gene Therapy* **2015**, *33*, 395.
[54] X. Ding, M. P. Stewart, A. Sharei, J. C. Weaver, R. S. Langer, K. F. Jensen, *Nat. Biomed. Eng.* **2017**, *1*, 0039.
[55] V. S. S. A Ayyadevara, K.-H. Roh, *Drug Deliv* **2020**, *27*, 805.
[56] T. Schlake, A. Thess, M. Thran, I. Jordan, *Cell. Mol. Life Sci.* **2019**, *76*, 301.
[57] H. Wang, B. Liu, J. Wei, *Cancer Lett* **2021**, *517*, 96.
[58] L. Raes, S. C. De Smedt, K. Raemdonck, K. Braeckmans, *Biotechnol. Adv.* **2021**, *49*, 107760.

[59] Invitrogen. Neon Transfection System Cell Protocols: Human T cells microporation. Published online 2009, 85888.
[60] Lonza Amaxa TM 4D-Nucleofector TM Protocol for Stimulated Human T Cells For 4D-Nucleofector TM, **2010**.
[61] P. Hsi, R. J. Christianson, R. A. Dubay, C. A. Lissandrello, J. Fiering, J. L. Balestrini, V. Tandon, *Lab Chip* **2019**, *19*, 2978.
[62] L. Chicaybam, A. L. Sodre, B. A. Curzio, M. H. Bonamino, *PLoS One* **2013**, *8*, 1.
[63] J. Loo, B. Chang, T. Dunn, et al., Microfluidic-Enabled Delivery of mRNA into PBMCs for Multiplex Transfection of Naïve T Cell, Natural Killer Cell, and Other Lymphocytes. Am Soc Cell Gene Ther 2021 Conf Proc.:1.
[64] J. Yen, M. Fiorino, Y. Liu, et al., *Sci. Rep.* **2018**, *8*, 1.
[65] D. Gurusamy, A. N. Henning, T. N. Yamamoto, Z. Yu, N. Zacharakis, S. Krishna, R. J. Kishton, S. K. Vodnala, A. Eidizadeh, L. Jia, C. M. Kariya, M. A. Black, R. Eil, D. C. Palmer, J. H. Pan, M. Sukumar, S. J. Patel, N. P. Restifo, *Cancer Cell* **2020**, *37*, 818.
[66] J. Eyquem, J. Mansilla-Soto, T. Giavridis, S. J. C. Van Der Stegen, M. Hamieh, K. M. Cunanan, A. Odak, M. Gönen, M. Sadelain, *Nature* **2017**, *543*, 113.
[67] A. Seki, S. Rutz, *J. Exp. Med.* **2018**, *215*, 985.
[68] F. Ahmadi, A. B. V. Quach, S. C. C. Shih, *Biomicrofluidics* **2020**, *14*, 061301.
[69] P. C. Gach, K. Iwai, P. W. Kim, N. J. Hillson, A. K. Singh, *Lab Chip* **2017**, *17*, 3388.
[70] P. C. Gach, S. C. C. Shih, J. Sustarich, J. D. Keasling, N. J. Hillson, P. D. Adams, A. K. Singh, *ACS Synth. Biol.* **2016**, *5*, 426.
[71] E. Moazami, J. M. Perry, G. Soffer, M. C. Husser, S. C. C. Shih, Shih SCC. Integration of World-to-Chip Interfaces with Digital Microfluidics for Bacterial Transformation and Enzymatic Assays. Anal Chem. Published online 2019:acs.analchem.8b05754. doi:10.1021/acs.analchem.8b05754.
[72] H. Wang, L. Chen, *Nanotechnol Rev* **2021**, *10*, 857.